R. Steger
K. Lin
Mechanical Engineering Department,
University of California,
Berkeley, CA 94720

B. D. Adelstein
Human Factors Research & Technology Division,
NASA Ames Research Center,
Moffett Field, CA 94035

H. Kazerooni
Mechanical Engineering Department,
University of California,
Berkeley, CA 94720

Design of a Passively Balanced Spatial Linkage Haptic Interface

This paper describes the design and implementation of a compact high fidelity desktop haptic interface that provides three-degree-of-freedom point-force interaction through a handheld pen-like stylus. The complete haptic device combines a spatial linkage, actuation, power amplification, and control electronics in a standalone package with a footprint similar to that of a notebook computer (33 cm×25 cm×10 cm). The spatial linkage is composed of one planar and two spherical subloops. Two versions of the spatial linkage were designed: a lightweight polycarbonate plastic version suitable for inexpensive mass production, and an aluminum and stainless steel linkage that offers greater reliability and higher stiffness. Both linkages were designed to be statically balanced over their full workspace. [DOI: 10.1115/1.1798111]

1 Introduction

1.1 Objective. Our goal was to create a portable self-contained haptic device for precision finger-scale interaction that could enable point force interaction over a three-dimensional translational work volume. The device is a desktop unit intended to provide a haptic interface to personal computer (PC) based virtual environments (Fig. 1). Through the use of a unique kinematic linkage [1], we sought to create a haptic device with capabilities equal to or better than those available in commercially available haptic interfaces.

Because the purpose of a haptic device is to simulate the forces generated through interaction with physical objects, performance is typically measured by the level of realism achieved. Guidelines for obtaining a realistic haptic simulation include multiple degrees of freedom, human matched force capability, low friction, near-zero backlash, and gravitational counterbalancing [2]. The present joystick design addresses these points and offers exceptionally smooth force output, low inertia resulting in a high motion bandwidth, and high motion resolution. Our design goal is to provide a single unit standalone desktop haptic interface device that combines high performance with portability and low cost to manufacture.

1.2 Background. While some of the earliest haptic devices date back to 1940's nuclear materials handling equipment [3], the first computer-controlled joystick-type haptic devices were not developed until the early 1970's [4]. With the rapid increase in the availability of inexpensive and accessible computing power, dozens of designs have emerged in the past decade. Through application of a previously patented kinematic linkage architecture [5], we sought to create a haptic device with capabilities comparable in many respects to those currently available commercial haptic interfaces like the popular PHANToM Haptic Interface, produced by SensAble Technologies [6]. The performance specifications of the original PHANToM (model: "Premium 1.0") set the following targets for realistic simulation of precision finger-scale manipulation: less than 0.1 N static backdrive friction, inertia such that the user perceives unbalanced weight of 0.2 N or less, maximum stiffness of 35 N/cm, peak and continuous end effector forces of 10 and 1.5 N, respectively, and end effector spatial resolution of at least 400 dpi (98 μm) [6]. Like many of its predecessors, the PHANToM makes at least partial use of serial elements as part of the force transmitting mechanism. A purely serial mechanism employs a single path to connect its base link to its terminal link. In this configuration, proximal links (links closer to the base) in a chain are required to carry and move the more distal links (those closer to the end point) and their actuators, resulting in increased linkage inertia and decreased linkage stiffness.

Conversely, a parallel mechanism joins its base and terminal links across multiple pathways. In the case of our joystick, its links are arranged in a fully parallel mechanism that enables fixing all of the actuators to ground, significantly reducing the system inertia. Moreover, because a parallel mechanism uses multiple pathways arranged in one or more closed kinematic loops, the resulting device can be made to have higher stiffness than serial mechanisms, which in turn allows high bandwidth force transmission. Other haptic devices that make use of a parallel configuration include Gough–Stewart platform-like haptic devices [7–9], wire actuated [10–12], and spherical linkage mechanisms [13,14] similar to the scheme chosen for our design.

For several years, UC Berkeley and NASA Ames have collaborated on the development of joystick-type haptic devices based on a common underlying parallel planar-spherical spatial kinematic architecture [1]. The haptic device described in this paper represents the most recent iteration in this research. The first joystick produced used a large set of links and provided for full arm-scale motion in the joystick workspace [15]. This device was later scaled down to provide a workspace compatible with the smaller finger and hand motions similar to those performed when using a writing instrument or a computer mouse [16]. In a subsequent project, further refinements were made to the control electronics to improve motion resolution and provide a smoother "feel" to the simulated forces [17,18]. The current joystick maintains the finger-motion-sized workspace and improves both the joystick linkage design and the control hardware and software.

These joystick devices have been used in haptic demonstrations in our labs. We have also used one of these devices in an investigation of texture perception [15,19]. The new metal joystick described in this paper is intended for ongoing human performance research at NASA Ames.

2 Device Overview

The joystick linkage (Fig. 2) contains 10 rigid links with 12 revolute joints, in a parallel spherical mechanism arranged in three closed kinematic loops. The device provides point-force interaction over a three-dimensional translational work volume and has evolved from previous joysticks designed in our lab [1]. The joystick is manipulated through various styli that attach to a magnetic ball joint on the endpoint. The links are passively mass balanced so gravity forces cannot be felt by the user as the end effector is moved.

Contributed by the Mechanisms and Robotics Committee for publication in the JOURNAL OF MECHANICAL DESIGN. Manuscript received August 12, 2003; revised February 6, 2004. Associate Editor: M. Raghavan.

Fig. 1 Finished three-degree-of-freedom fused deposition modeling (FDM) rapid prototype polycarbonate joystick. The actuators, power amplifiers and control electronics are all housed in the enclosure. The complete haptic device dimensions are 33 cm×25 cm×10 cm.

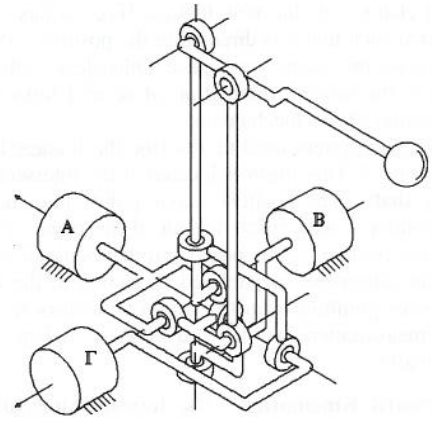

Fig. 3 Simplified view of the original joystick linkage from Ref. [1]. This configuration is kinematically equivalent to the new linkage design.

Actively controlled force is provided by three brushless direct current (dc) motors with housings fixed to the joystick enclosure so the linkage does not carry their weight. Open loop force and motion transfer fidelity is improved due to the lack of transmission elements (such as gears or cable drives) that would otherwise increase friction and add backlash. Sinusoidally wound, brushless dc motors are used to provide up to 5 N of force at the joystick endpoint for short durations (2 s, based on amplifier and motor specifications). Because sinusoidal motor commutation is matched to the motor winding profile, torque ripple (spatially dependent periodic deviations from commanded actuator torque) is eliminated, providing smooth feeling surfaces during joystick simulations. The use of analog sinusoidal encoders and sinusoidal interpolation provides high-resolution angular position feedback from the motors.

Software has been written to provide communication between the joystick and an external PC through a standard parallel port interface. Testing on the prototype hardware has confirmed a maximum frame rate of 1.5 kHz (1500 packets of information per second). Since each packet includes 700 bits of data, the data rate to PC is approximately 1 Mbps. This communication allows the joystick endpoint position and velocity data to be sent from the joystick to the PC to update a virtual environment and a force command to be sent from the PC virtual environment to the joystick to be felt by the user.

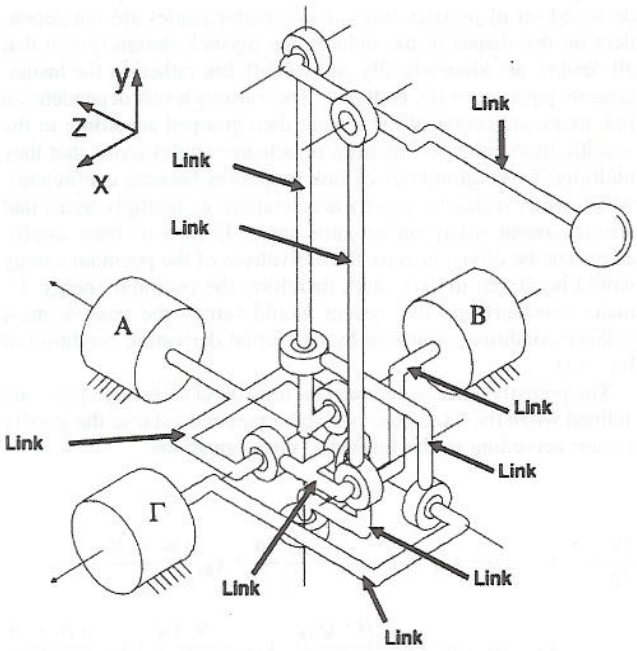

Fig. 2 Plastic linkage assembly: each link is labeled and motor axes α, β, and γ are shown (Link 1 is the stationary base link formed by the enclosure and is not shown. This base link lies in the plane of the motor axes).

3 Kinematics Overview

For a full derivation of the joystick kinematics, the reader should refer to Adelstein, Ho, and Kazerooni [1]. This section is intended to familiarize the reader with the mechanism and cover the forward kinematics and the instantaneous Jacobian used in the control software. The forward kinematics convert actuator angle measurements into end effector Cartesian space while Jacobian transforms end effector forces in Cartesian space into desired actuator torques.

The joystick mechanism consists of two spherical loops and one planar loop. The first loop is links 1, 2, 3, 4, and 5 and the second is links 5, 6, 7, 8, and 1. (See Fig. 2 for the full linkage assembly and link labeling.) These two loops form a spherical linkage because the axes of all its joint axes at one common point. The final loop, comprising links 4, 5, 6, 10, and 9, forms a planar parallelogram structure.

The shape of the links has been changed significantly from our previous implementations to attain the mass balance and workspace improvements discussed later in this paper; however the relative locations of the revolute joints has not changed. The new linkage is kinematically equivalent to the simplified sketch of the original linkage architecture shown in Fig. 3. One of the most

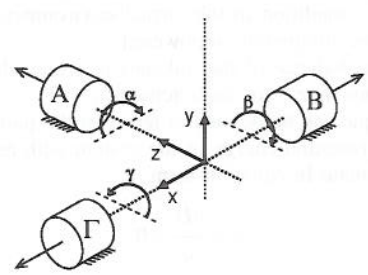

Fig. 4 The coordinate system used to describe the joystick linkage kinematics. Positive angular (α, β, and γ) and translational (x, y, and z) displacement are labeled. Actuators are labeled A, B, and Γ. The origin of the xyz coordinate frame is located at the mechanism center of the spherical portion of the linkage.

pronounced changes is that new linkage (Fig. 2) has the end effector inverted such that it is directed in the positive z direction in order to increase the usable workspace. Other less visible changes were made to the relative orientation of several links within the spherical portion of the mechanism.

The coordinate system used to describe the linkage kinematics is shown in Fig. 4. The origin is located at the intersection of the three motor shafts. The positive x-axis points into the Γ motor shaft, the positive y-axis points up out of the plane of the motor shafts, and the positive z-axis points into the A motor shaft. Positive angle measurements are defined according to the right hand rule about axes pointing from the origin to motors A, B, and Γ. Zero angle measurements are defined as the x-z plane containing the motor shafts.

3.1 Forward Kinematics. The forward kinematics of the linkage map the joint angles of the actuators to the Cartesian coordinates of the end effector and are shown in Eq. (1)–(3). The end effector position of the joystick is given by the x, y, and z coordinates for the actuator angles α, β, and γ

$$x=\left[\frac{L_1\ s\alpha\ c\beta}{d_\beta}+\frac{L_2\ s\alpha\ c\gamma}{d_\gamma}\right] \tag{1}$$

$$y=\left[\frac{L_1\ c\alpha\ c\beta}{d_\beta}+\frac{L_2\ c\alpha\ c\gamma}{d_\gamma}\right] \tag{2}$$

$$z=\left[\frac{-L_1\ c\alpha\ s\beta}{d_\beta}+\frac{L_2\ c\alpha\ s\gamma}{d_\gamma}\right] \tag{3}$$

where $d_\beta=\sqrt{1-s^2\alpha s^2\beta}$ (4)

$$d_\gamma=\sqrt{1-s^2\alpha s^2\gamma} \tag{5}$$

$$sx=\sin(x) \tag{6}$$

$$cx=\cos(x) \tag{7}$$

and L_1 is the upper arm length, along link 6 between its joints with link 5 and link 10. L_2 is the forearm length, along link 10 between its joints with links 6 and the end effector. Together, in this particular implementation, links 4, 6, 9, and 10 define the sides of the parallelogram. By choosing lengths L_1 and L_2 to be equal, the singularities of the parallel mechanism lie only in the x-z plane and at the surface of the workspace hemisphere. Also, this choice simplifies the calculation of the system Jacobian.

3.2 Jacobian. The system Jacobian relates the endpoint force to the actuator torque in the following relationship:

$$J^T\begin{bmatrix}F_x\\F_z\\F_y\end{bmatrix}=\begin{bmatrix}T_\alpha\\T_\beta\\T_\gamma\end{bmatrix} \tag{8}$$

where $[F_x\ F_y\ F_z]^T$ is the vector of endpoint force in the Cartesian coordinates and $[T_\alpha\ T_\beta\ T_\gamma]^T$ is the vector actuator torque in the motor coordinates shown in Fig. 4. The partial derivative of Eqs. (1)–(3) with respect to α, β, and γ, gives the linkage system's Jacobian [1]:

$$J=\frac{1}{d_\beta^3\ d_\gamma^3}\begin{bmatrix}-(L_1\ d_\gamma^3\ c\alpha\ c\beta+L_2\ d_\beta^3\ c\alpha\ c\gamma) & L_1\ d_\gamma^3\ s\alpha\ c^2\alpha\ s\beta & L_2\ d_\beta^3\ s\alpha\ c^2\alpha\ s\gamma\\ -(L_1\ d_\gamma^3\ s\alpha\ c^3\beta+L_2\ d_\beta^3\ s\alpha\ c^3\gamma) & -L_1\ d_\gamma^3\ c^3\alpha\ s\beta & -L_2\ d_\beta^3\ c^3\alpha\ s\gamma\\ -(L_1\ d_\gamma^3\ s\alpha\ s\beta\ c^2\beta fl_2\ d_\beta^3\ s\alpha\ s\gamma\ c^2\gamma) & -L_1\ d_\gamma^3\ c\alpha\ c\beta & L_2\ d_\beta^3\ c\alpha\ c\gamma\end{bmatrix} \tag{9}$$

where, for this implementation

$$L_1=L_2=L \tag{10}$$

and Eqs. (4) and (5) define $d\beta$ and $d\gamma$.

4 Passive Mass Balance

Balancing the linkage of a haptic device provides a lighter feel to virtual environment simulations because the user does not need to provide a supporting force and has been used extensively in robotics [20]. By balancing the linkage passively (as opposed to an active balance that relies on power from the actuators [21]), we are able to reduce computational burden for the embedded processor. Also, the passive balance allows for a truly smooth simulation of a zero-force condition in the virtual environment because the actuators can be completely unpowered.

Passive mass balance of the linkages is achieved if the torque induced by gravity, τ_i, for each actuator ($i=1,\ldots,3$) is always zero. This torque can be defined in terms of the partial derivative of the gravity potential energy of the system with respect to each actuator coordinate In equation form

$$\tau_i=\frac{\partial U}{\partial q_i}=0 \tag{11}$$

where U is the potential energy of the whole system and q_i is the ith system coordinate. Equation (11) will be satisfied if the derivatives of U are forced to be constant for all q_i. The equations for the potential energy, U, are expressed in terms of the mass and location of the mass center for each link and its attached counterweights in the local link coordinate frame and the displacement of the link mass centers above a fixed inertial as a function of actuator angles. The mass and center of mass location are specific to the designed set of joystick links. The actuator angles are not dependent on the shapes of the links in the joystick design (given that all designs are kinematically equivalent), but rather on the instantaneous position of the endpoint. The various terms dependent on link mass and center of mass were then grouped according to the specific trigonometric functions of actuator angles terms that they multiply. These groupings of link properties become coefficients, which when scaled by gravity acceleration, g, multiply terms that are dependent solely on actuator angle. If each of these coefficients can be driven to zero, the derivatives of the potential energy would be driven to zero (and, therefore, the potential energy, U, made constant) and the system would satisfy the passive mass balance condition expressed by the partial derivative condition of Eq. (11).

The potential energy derivatives, regardless of linkage pose, are defined when the fixed base is aligned perpendicular to the gravity vector, according to the following three equations:

$$\begin{aligned}\frac{\partial U}{\partial\alpha}=&-k_{2y}\ s\alpha+k_{6y}\ c\alpha-k_{7y}\frac{c^3\beta\ s\alpha}{d_\beta^3}+k_{8y}\frac{c\alpha\ c^2\beta}{d_\beta^3}\\&-k_{9y}\ s\alpha\ c\alpha\ s\beta\frac{c^2\beta+Q_{ab}^2}{d_\beta^3}-k_{10y}\frac{c^3\gamma\ s\alpha}{d_\gamma^3}+k_{11y}\frac{c\alpha\ c^2\gamma}{d_\gamma^3}\\&-k_{12y}\ s\alpha\ c\alpha\ s\gamma\frac{c^2\gamma+Q_{ac}^2}{d_\gamma^3}\end{aligned} \tag{12}$$

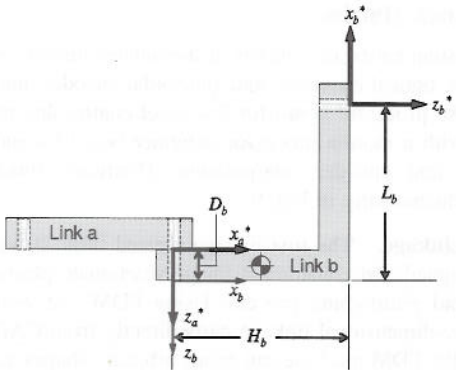

Fig. 5 The coordinate system used to define the link dimensions. In this example, D_b is greater than zero and for base links 2, 5, and 8 the origin frame (x_a^*, z_a^*) is at the mechanism center. Link pairs corresponding to *link a* and *link b* in this diagram are 3 and 2, 4 and 5, 6 and 5, and 7 and 8, respectively. For all planar links, L_b is equal to zero.

$$\frac{\partial U}{\partial \beta} = k_{4y}\ c\beta - k_{7y}\frac{s\beta\ c^3\alpha}{d_\beta^3}$$

$$\frac{\partial U}{\partial \gamma} = k_{5\gamma}\ c\gamma - k_{10\gamma}\frac{s\gamma\ c^3\alpha}{d_\gamma^3} \tag{13}$$

$$\text{where} \quad d_\beta = \sqrt{1 - s^2\alpha\ s^2\beta} \tag{14}$$

$$d_\gamma = \sqrt{1 - s^2\alpha\ s^2\gamma} \tag{15}$$

The coefficients used in Eqs. (12)–(13) are expanded later. They are subscripted y to acknowledge the vertical gravity vector as being in the y direction

$$k_{1y} = m_2 g y_2 \tag{16}$$

$$k_{2y} = m_5 g y_5 \tag{17}$$

$$k_{3y} = m_8 g y_8 \tag{18}$$

$$k_{4y} = m_2 g x_2 + m_3(D_3 + H_2 + z_3) \tag{19}$$

$$k_{5y} = m_7 g(D_7 + H_8 + z_7) + m_8 g x_8 \tag{20}$$

$$\begin{aligned} k_{6y} = {} & m_4 g(D_4 + H_5 + z_4) + m_5 g x_5 + m_6 g(D_6 + H_5 + z_6) \\ & + m_9 g(D_4 + D_9 + H_5 + z_9) \\ & + m_{10} g(D_{10} + D_4 + D_9 + H_5 + z_{10}) \end{aligned} \tag{21}$$

$$k_{7y} = m_3 g x_3 + m_4 g x_4 + m_9 g H_{4p} + m_{10} g(x_{10} + H_{4p}) \tag{22}$$

$$k_{8y} = m_3 g y_3 \tag{23}$$

$$k_{9y} = -m_4 g y_4 + m_{10} g y_{10} \tag{24}$$

$$k_{10y} = -m_6 g x_6 - m_7 g x_7 + m_9 g x_9 + m_{10} g H_9 \tag{25}$$

$$k_{11y} = -m_7 g y_7 \tag{26}$$

$$k_{12y} = m_6 g y_6 - m_9 g y_9 \tag{27}$$

where m_i is the mass of the ith link; g is the gravity x_i, y_i, and z_i are the coordinates of the center of mass of the ith link measured from the local link coordinate system; and the remaining variables are link dimensions. The link dimension coordinate systems are defined according to Fig. 5.

Seven of the coefficients defined in Eqs. (16)–(27) are immediately reduced to zero because of trivial symmetry when individual link centers of mass are located in the plane of the x-z axes of Fig. 5. (i.e., where $y_i = 0$). This leaves only coefficients k_{4y}, k_{5y}, k_{6y}, k_{7y}, and k_{10y}. In addition, although Eqs. (16)–(27) are derived for the case where the linkage base is horizontal, a solution to these equations can be shown to guarantee mass balance for all gravity vector orientations.

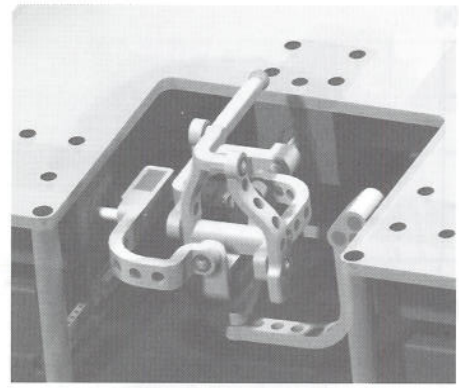

Fig. 6 CAD model close-up of the FDM plastic linkage assembly with mass-balance counterweights (shown installed in device encloser)

The values of each coefficient were calculated in a spreadsheet as link mass and dimensions and counterweight mass and placement were altered. At this stage it was decided that two different linkages would be designed. The first linkage (Fig. 6) was constructed from polycarbonate plastic parts on a fused deposition modeling (FDM) rapid prototyping system (Stratasys Inc., model: TITAN) in the laboratory at UC Berkeley. This linkage would not only be inexpensive to manufacture, but it would allow for the rapid construction and testing of several prototypes of the linkage. Brass extrusions were chosen as the counterweight material for their density, low cost, and ease of machining. In parallel, another version of the linkage was designed using a combination of 6061-T6 alloy aluminum and 304 alloy stainless steel for various links (Fig. 7) to fill the need for a durable research-grade device with higher stiffness.

Link dimension and counterweight location and center of mass were manually varied in an iterative process using the mass-balance spreadsheet and FDM prototypes to produce the final static balance. In addition, holes were bored through the non-counterweight portions of links to decrease the amount of counterweight mass needed as well as the overall system inertia. Tests with standard masses confirmed that the maximum vertical force required to support the unpowered linkage for the final designs was less than 0.02 N (2 g) for all endpoint locations tested within the workspace. After repeated design iterations, the residual force

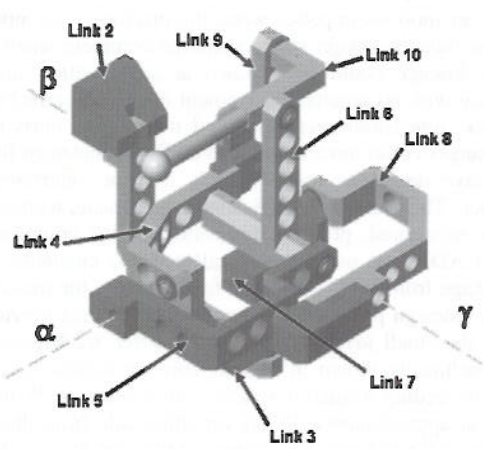

Fig. 7 CAD model of the metal implementation of spatial mechanism

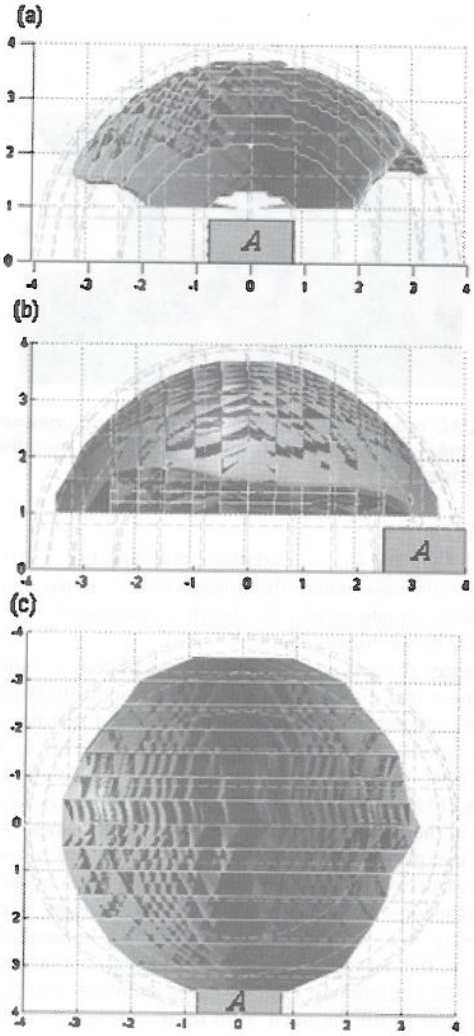

Fig. 8 ***(a–c)*** ***x-y, y-x,*** **and** ***x-z*** **plane views of the collision-free endpoint workspace. A rectangle, labeled** ***A,*** **represents the location of the alpha motor in each figure. All axes are labeled in inches. The origin in the figures is located at the mechanism center.**

associated with any remaining mass imbalance becomes insignificant when compared with the bearing friction and other imperfections associated with joint alignment and linkage dimension precision in the actual system. The friction and alignment related forces in the final joystick were sufficiently small that the user did not feel her motions impeded when the machine was unpowered. The mass balance design was considered complete when the unpowered linkage could be released at any position inside the workspace with no resultant movement of the end effector.

As link dimensions were modified to improve mass balance, these changes could have introduced collisions between links that would have decreased the joystick's useable, interference-free workspace. Therefore, as modifications were made, workspace extent was monitored, prior to fabrication on the computer aided design (CAD) parts using the visualNastran® kinematic simulation package from MSC Corp. The final result of the mass balance and link redesign provided a larger workspace than previous versions of the small joystick. The collision-free workspace for the metal machine is shown in Fig. 8. This workspace is a section slightly exceeding a quarter sphere with 9.5 cm (3.75 in.) outer radius, cut approximately 55 deg on either side from the vertical y-z plane of the linkage. The bottom of the workspace is bounded by a flat surface at the height of the base plate, parallel to the linkage system's x-z plane.

5 Joystick Hardware

The system hardware consists of the linkage, motors and power amplifiers, optical encoders, and sinusoidal encoder interpolators, and an x86 processor board for low-level control and haptic processing with a motion processor daughter board for motor commutation and encoder interpolation. Hardware functions are shown schematically in Fig. 9.

5.1 Linkage. The first linkage created (Fig. 2) was specifically designed and constructed for polycarbonate plastic and the FDM rapid prototyping process. Using FDM, we were able to print three-dimensional linkage parts directly from CAD models. Because the FDM machine can create arbitrary shapes and curves, a great deal of freedom in link design was possible without incurring a significant monetary cost or time increase in manufacturing. However, the penalty for using this material was greater linkage compliance due to the FDM plastic and poorer dimensional tolerance due to the 0.25 mm precision of the FDM machine, and brittleness which made the sections of the links near the bearings and couterweights prone to crack during assembly.

Because the FDM process builds parts by extruding a fine filament of molten plastic to fill in successive cross sections of the part, the finished product is highly anisotropic in its mechanical properties. Through our prototyping and testing process, we found the FDM parts not only tend to be weakest in the build plane of the part, but they also have a strong sensitivity to the pattern used to layout the filament in each layer of the part. Each linkage part was designed with a particular FDM build orientation in order toprovide best strength. In addition, many of the parts required specifying the fill pattern of the plastic filament for every layer in the part. These steps are not typically necessary in large FDM parts where the layer thickness and size of the FDM filament are very small in comparison to the part as a whole.

The counterweights for the mass balance of the FDM version were designed to be simple rectangular prisms or cylinders for manufacturability. Thus, the counterweights could be cut from standard size extruded brass sections. Each revolute joint in the linkage was constructed using a steel shaft and a pair of ABEC grade 5 shielded, flanged, radial ball-bearings bonded in place in the FDM part. Various graspable stylus designs can be connected to the ball via a low friction magnetic ball joint that is coupled to the endpoint (at link 10) of the joystick linkage.

The second implementation of the linkage, seen in Fig. 7, used aluminum for the links and stainless steel for the counterweights. The all-metal construction enabled tolerances significantly better than the 0.25 mm of the FDM process. The precision and stiffness of this design made it more suitable for use in the human performance experiments.

However, the higher manufacturing cost makes the design less appealing commercially. It should also be noted that FDM and metal linkages were designed to be interchangeable, such that both could use the same base assembly, control, and actuation, with no need to modify the hardware or software.

5.2 Sinusoidal Encoders. The encoders, which provide the angular position for each motor shaft, have incremental 1024 line sinusoidal output (Computer Optical Inc.; model CP-5150). Each encoder generates two channel quadrature (i.e., with 90° relative phase shift) differential analog signals that vary sinusoidally for each line on the encoder disk. A transistor–transistor logic level index pulse, which was aligned to the respective motor's windings, is also generated by each encoder.

An encoder interpolator module (Computer Optical Inc.; model CP-1064-16-1) added to each encoder performs 64X sine interpolation and outputs a standard quadrature signal. With this sine interpolation, and 4X quadrature decoding, the angular position

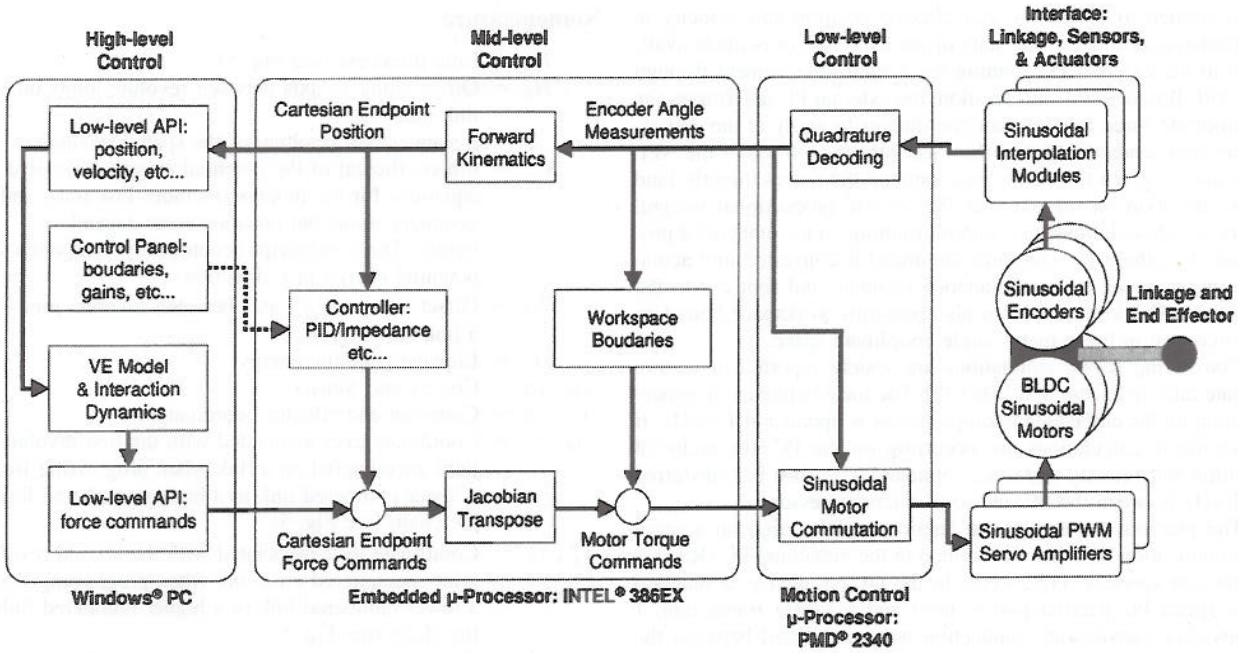

Fig. 9 Control hardware and software architecture

resolution information is $1024 \times 16 \times 4 \approx 65.5$ K counts/rev. At the joystick endpoint's maximum reach of 10 cm, this corresponds to a theoretical resolution in x-y-z endpoint space of 9.6 μm. The actual resolution of the endpoint position is coarser due to factors such as compliance of the links and joints.

5.3 Motors and Amplifiers. The joystick uses brushless dc motors (Pittman Motors; ELCOM model 4141). The motors have four-pole, three-phase slotless sinusoidal windings. The motors were chosen because they provide a constant torque profile when commutated sinusoidally, a high torque to size ratio, and low inertia. At its rated continuous torque, the motor produces approximately 1.4 N (measured) at the end effector when the linkage is fully extended to its maximum 10 cm reach. This force level is sufficient to cover the majority of precision finger-scale manipulation tasks [5]. In addition, a peak force of 5 N can be applied for durations less than 2 s (duration limited by the amplifiers).

Compact sinusoidal pulse width modulated (PWM) amplifiers (Advanced Motion Controls; model S16A8) provide a maximum 8 A of current per motor (or 75 W per motor based on the motor winding resistance). The PWM amplifiers switching frequency is 33 kHz, well above the 20 kHz human audible range and beyond the mechanical bandwidth of the system.

The three motors and amplifiers are contained within the desktop joystick housing. The top and bottom plate, onto which the motors and amplifiers are respectively mounted, also serve as heat sinks.

6 Control Hardware

The control architecture for the haptic joystick is divided between a midlevel embedded x86 based microprocessor and a low-level dedicated motion control chip. Together, they form a standalone controller that is housed inside the joystick base enclosure along with the motors and servo amplifiers. The control architecture is shown in Fig. 9.

6.1 Midlevel Control: Embedded Microprocessor. The midlevel control is performed by the embedded Intel 386EX microprocessor on development board from Tern Inc. (model: i386-Engine). The midlevel board is responsible for the servo control function that calculates the commanded interaction forces and the workspace boundary enforcement function that prevents motion into regions where link interference would occur. The midlevel control also includes a communication interface to an optional external computer that can run virtual environment simulations.

6.2 Low-Level Control: Motion Processor. The low level control is carried out on the Tern MotionC-S development board with PMD Navigator® Series motion processor. The motion processor performs quadrature decoding to give angular position for each axis. It also estimates velocity by keeping track of the number of encoder counts over a known time window. The low-level embedded controller can vary the size of this window to improve the velocity estimate for slow motions. The PMD chip is also responsible for the sinusoidal motor commutation, producing ripple-free torque control of the sinusoidally wound motors.

7 Software

The joystick appears to the user as an impedance-controlled device. Under impedance control, the input is the motion of the endpoint generated by the human. This motion is sensed by the device's encoders and transformed to motion of a virtual endpoint in a virtual environment running on either the embedded processor or an external personal computer. The output signal (feedback) to the user is the point force generated by the joystick at its end effector. Our device is intended to interface with existing virtual environment software for the PC. This virtual environment software determines what force should be generated at the end effector based on its location in the virtual environment. For example, if the end effector in the virtual environment were to strike a virtual "wall," a force could be generated that is proportional to the depth of penetration of the virtual wall. We also developed a simple application program interface (API) for the PC to interface the haptic device controller to PC virtual environment software. The API includes functions to obtain the end effector position and velocity as well as output a three-component force vector at end effector force. This way the virtual environment developer can utilize the API to create new Microsoft Windows applications that incorporate the relationship that best fits the experiment or haptic environment she is trying to create.

The software architecture is shown in Fig. 9. The local (midlevel) processor converts the encoder counts for each actuator axis into angle measurements. The forward kinematic relations are

then applied to obtain the end effector position and velocity in Cartesian coordinates. The state of the end effector is made available to the external PC running the virtual environment through the API. Based on this information, the external PC determines the appropriate force in Cartesian coordinates to apply at the end effector and sends this out to the local processor through the API. The user is given the option to command the forces directly (and close the loop on the external PC) or use proportional integral derivative-based impedance control running on the embedded processor. In either case, the force command is converted into actuator torques using the instantaneous Jacobian and sent out to the actuators. The local processor also performs workspace boundary enforcement in the actuator angle coordinate space.

Convincing haptic simulations are widely reported to require update rates in excess of 1 kHz [22]. The local haptic environment running on the embedded microprocessor is updated at 1.5 kHz. If other haptic calculations are occurring on the PC, the endpoint position and velocity and force command data must be transferred at 1 kHz between the PC and local microprocessor.

The previous version of the haptic joystick relied on a serial communication link that was limited to the maximum PC (RS232) serial port speed of 115.2 kbps. In the present device, a standard high speed PC parallel port is used and a 1 kHz frame rate, 1 Mbps data transfer rate connection was established between the PC and the haptic device. This is intentionally made less than the maximum data rate achieved in testing to guarantee performance in the Windows PC environment. While the universal serial bus (USB) has become a standard high-speed interface for PCs and seems like a promising technology for haptic communication, it does so by transmitting large blocks of data at a fairly slow rate (a maximum of 500 Hz. for the USB 1.1) [23]. USB 2.0, with a frame rate eight times higher than USB 1.1, could allow for a 1 kHz haptic communication; was not available at the time our system was developed.

8 Conclusions

We have designed a three-degree-of-freedom force-feedback haptic joystick with goal of combining portability and compact size with the performance (spatial resolution, continuous force magnitude, smoothness, balance, and haptic update rate) necessary for precision finger-based interaction. The current iteration of the joystick uses links kinematically equivalent to past versions. However, the new design provides a larger workspace and is passively mass balanced.

Two versions of the mechanical linkage were prototyped: a low cost FDM polycarbonate linkage potentially suitable for mass production and a precision all-metal linkage designed for haptics research. However, because of dimensional imprecision and excessive compliance, further development of the FDM version has been postponed for now.

Software has been written to allow for high-speed data transfers between the joystick and the PC. A simple API is also provided to allow the haptic device to interact with other virtual environment software. The function of individual device subsystems have thus far been tested separately. We expect shortly to being the process of integrating the communication software and API with the low-level control code on the embedded platform and connect the control system to the actuated linkage. Testing of the completed hardware and software system will follow.

Acknowledgments

Work at UC Berkeley was supported by NASA-ARC Cooperative Agreement No. NCC2-1347 with funding from the NASA Intelligent Systems Human Centered Computing Program and a NASA-Ames Director's Discretionary Fund Award.

Nomenclature

D_b = Link thickness (see Fig. 5)

H_b = Offset along x_b axis between revolute joints on a link (see Fig. 5)

J = Instantaneous Jacobian of the spatial linkage

K_{ny} = nth coefficient of the potential energy derivative equations for the linkage (includes link mass and geometry terms but no orientation dependant terms). The y subscript denotes only components of potential energy in y direction

L_b = Offset along the x_b^* axis between revolute joints on a link (see Fig. 5)

U = Linkage potential energy

cn, sn = Cos(n) and Sin(n)

x, y, z = Cartesian end effector coordinates

x_b, z_b = Coordinate axes associated with the first revolute joint encountered on a link when progressing from a lower numbered link to a higher numbered link in the chain (see Fig. 5).

x_b^*, z_b^* = Coordinate axes associated with the second revolute joint encountered on a link when progressing from a lower numbered link to a higher numbered link in the chain (see Fig. 5).

A, B, Γ = Three dc motor actuators in the haptic device

α, β, γ = Axes associated with actuators A, B, and Γ, also represents angle of actuator rotation for each axis

References

[1] Adelstein, B. D., Ho, P., and Kazerooni, H., 1996, "Kinematic design of a three degree of freedom parallel hand controller mechanism," *Proc. 5th Symposium on Haptic Interfaces for Virtual Environment and Teleoperator Systems, ASME Dynamic Systems and Control Division*, DSC-Vol. 58, New York, pp. 539–546.

[2] Millman, P. A., and Colgate, J. E., 1991, "Design of a four degree-of-freedom force reflecting manipulandum with a specified force/torque workspace," *Proc. IEEE Conference on Robotics and Automation*, Sacramento, pp. 1488–1493.

[3] Goertz, R. C., and Thompson, W. M., 1954, "Electronically controlled manipulator," Nucleonics, pp. 46–47.

[4] Batter, J. J., and Brooks, Jr., F. P., 1971, "A computer display to the sense of feel," *Information Processing, Proc. IFIP Congress 71*, Ljubljana, pp. 506–508.

[5] Adelstein, B. D., 1998, "Three degree of freedom parallel mechanical linkage," U.S. Patent No. 5,816,105.

[6] Massie, T. H., and Salisbury, J. K., 1994, "The PHANToM haptic interface: A device for probing virtual objects," *Symposium on Haptic Interfaces for Virtual Environment and Teleoperator Systems, Proc. ASME Dynamic Systems and Control Division*, DSC-Vol. 55-1, New York, pp. 295–301.

[7] Siva, K. V., Dumbreck, A. A., Fischer, P. J., and Abel, E., 1988, "Development of a general purpose hand controller for advanced teleoperation," *Proc. International Symposium on Teleoperation and Control*, Bristol, pp. 277–290.

[8] Brandt, G., Aimlong, A., Carrat, L., Merloz, P., Staudte, H. W., Lavallee, S., Radermacher, K., and Rau, G., 1999, "CIRGOS: A compact robot for image guided orthopaedic interventions," IEEE Trans. Inf. Technol. Biomed., **3–4**, pp. 252–260.

[9] Grange, S., Conti, F., Helmer, P., Rouiller, P., and Baur, C., 2001, "Overview of the Delta Haptic Device (poster)," *Eurohaptics 2001*, Birmingham, England.

[10] Melchiorri, C., Vassura, G., and Arcara, P., 1999, "What kind of haptic perception can you get with a one-wire interface?," *Proc. IEEE Conference on Robotics and Automation*, Detroit, pp. 1620–1625.

[11] Takeda, Y., and Funabashi, H., 2000, "Kinematic synthesis of spatial inparallel wire-driven mechanism with six degrees of freedom with high force transmissibility," *Proc. ASME 2000 Design Engineering Technical Conferences*, Baltimore, pp. 1–9.

[12] Kim, S., Ishii, M., Koike, Y., and Sato, M., 2000, "Development of tension Based haptic interface and possibility of its application to virtual reality," *Proc. ACM Symposium on Virtual Reality Software and Technology*, pp. 199–205.

[13] Birglen, L., Gosselin, C., Pouliot, N., and Monsarrat, B., 2002, "SHaDe, A new 3-DOF haptic device," IEEE Trans. Rob. Autom., **18-2**, pp. 166–175.

[14] Adelstein, B. D., and Rosen, M. J., 1992, "Design and implementation of a force reflecting manipulandum for manual control research," ASME Advances in Robotics, **42**, pp. 1–12.

[15] Ho, P., 2002, "Haptic simulation of 3D primitive objects and textures using a novel force-reflecting interface," Ph.D. thesis, University of California, Berkeley, Berkeley, CA.

[16] Adelstein, B. D., Gayme, D. F., Kazerooni, H., and Ho, P., 1998, "Three degree of freedom haptic Interface for precision manipulation," *Proc. ASME Dynamic Systems and Control Division*, DSC-Vol. 64, New York, p. 185.
[17] Chung, R., 2001, "Actuator, sensor, and control hardware for improved haptic interface performance," Masters of Science thesis, University of California, Berkeley, Berkeley, CA.
[18] Chung, R., 2002, "Hardware for improved haptic interface performance," in *Touch in Virtual Environments: Haptics and the Design of Interactive Systems*, edited by M. L. McLaughlin, J. P. Hespanha, and G. S. Sukhatme, Prentice Hall, Upper Saddle River, NJ, pp. 71–94.
[19] Ho, P., Adelstein, B. D., and Kazerooni, H., 2004, "Judging 2D versus 3D square-wave virtual gratings," *Proceedings, 12th International Symposium on Haptic Interfaces for Virtual Environment and Teleoperator Systems*, IEEE, Chicago, pp. 176–183.
[20] Ebert-Uphoff, I., Gosselin, C. M., and Laliberte, T., 2000, "Static balancing of spatial parallel platform mechanisms—Revisited," ASME J. Mech. Des., **122**, pp. 43–51.
[21] Yu, Y., and Lin, J., 2003, "Active balancing of a flexible linkage with redundant drives," ASME J. Mech. Des., **125**, pp. 119–123.
[22] Marcus, C. E., 1998, "Force feedback for surgical simulation," Proc. IEEE, **86**, pp. 524–530.
[23] Anderson, D., 2001, *Universal Serial Bus System Architecture*, 2nd ed., edited by K. Tibbetts, pp. 13–24.